Available online at www.sciencedirect.com
ScienceDirect
Biochimica et Biophysica Acta 1777 (2008) 239–249
Biochimica et Biophysica Acta BBA
www.elsevier.com/locate/bbabio

Mutations in cytochrome *b* that affect kinetics of the electron transfer reactions at center N in the yeast cytochrome bc_1 complex

Frederik A.J. Rotsaert, Raul Covian, Bernard L. Trumpower *

Department of Biochemistry, Dartmouth Medical School, 7200 Vail, Hanover, New Hampshire 03755, USA

Received 6 July 2007; received in revised form 15 August 2007; accepted 17 August 2007
Available online 6 September 2007

Abstract

We have examined the pre-steady-state kinetics and thermodynamic properties of the *b* hemes in variants of the yeast cytochrome bc_1 complex that have mutations in the quinone reductase site (center N). Trp-30 is a highly conserved residue, forming a hydrogen bond with the propionate on the high potential *b* heme (b_H heme). The substitution by a cysteine (W30C) lowers the redox potential of the heme and an apparent consequence is a lower rate of electron transfer between quinol and heme at center N. Leu-198 is also in close proximity to the b_H heme and a L198F mutation alters the spectral properties of the heme but has only minor effects on its redox properties or the electron transfer kinetics at center N. Substitution of Met-221 by glutamine or glutamate results in the loss of a hydrophobic interaction that stabilizes the quinone ligands. Ser-20 and Gln-22 form a hydrogen-bonding network that includes His-202, one of the carbonyl groups of the ubiquinone ring, and an active-site water. A S20T mutation has long-range structural effects on center P and thermodynamic effects on both *b* hemes. The other mutations (M221E, M221Q, Q22E and Q22T) do not affect the ubiquinol oxidation kinetics at center P, but do modify the electron transfer reactions at center N to various extents. The pre-steady reduction kinetics suggest that these mutations alter the binding of quinone ligands at center N, possibly by widening the binding pocket and thus increasing the distance between the substrate and the b_H heme. These results show that one can distinguish between the contribution of structural and thermodynamic factors to center N function.

Keywords: bc_1, complex; Cytochrome *b*; Kinetics; Protonmotive Q cycle; Yeast

1. Introduction

The cytochrome bc_1 complex is an energy transducing integral membrane enzyme that links the transfer of electrons from ubiquinol to cytochrome *c* to proton translocation across the membrane via the protonmotive Q cycle [1,2]. In the absence of a protonmotive force to provide energy, the quinol oxidation reaction at center P is essentially irreversible, and the two electrons from quinol follow divergent pathways through the bc_1 complex. One electron is transferred to the high potential acceptors, the Rieske iron–sulfur protein and cytochrome c_1. The second electron from quinol oxidation enters the low potential chain in cytochrome *b* through the low potential *b* heme (b_L heme) and than transfers to the high potential heme (b_H heme) at center N, where it reduces quinone to form a stable semiquinone. A second quinol oxidation reaction at center P completes the cycle with the reduction of semiquinone to quinol at center N.

In order for the b_H heme to reduce both quinone and semiquinone the semiquinone must be stabilized so that the reduction potentials required for the two electron transfer reactions are not significantly different. However, the structural basis of semiquinone stabilization at center N is not presently clear. We previously proposed that inter-monomer communication through the b_L heme might be important [3,4]. In addition, thermodynamic factors such as the redox potential of the b_H heme together with different binding affinities for the quinone ligands may also contribute to the presence of semiquinone as a long-lived intermediate at center N [5]. The availability of a high-resolution structure of the yeast bc_1 complex [6] allows the opportunity to revisit some previously reported center N mutants

Abbreviations: b_L heme, Low potential *b* heme; b_H heme, High potential *b* heme

* Corresponding author. Tel.: +1 603 650 1621; fax: 1 603 650 1128.
E-mail address: Trumpower@Dartmouth.edu (B.L. Trumpower).

0005-2728/$ - see front matter © 2007 Elsevier B.V. All rights reserved.
doi:10.1016/j.bbabio.2007.08.005

[7,8] in order to elucidate the relative contribution of thermodynamic and structural parameters to center N function.

In the present study we have examined the bc_1 complexes from seven center N yeast mutants. These were obtained as revertants of respiratory-deficient yeast strains [9,10] or as mutations that conferred resistance towards ilicicolin H, a novel center N inhibitor [7]. All of the mutants exhibited normal growth on non-fermentable carbon sources and normal cytochrome *c* reductase activities of the mitochondrial membranes. The pre-steady-state reduction kinetics of the bc_1 complexes isolated from these mutants were examined in the presence of inhibitors that differentiate reduction of cytochrome *b* through center P and center N. The results are discussed with respect to the thermodynamic properties of the b_H heme and binding affinity of center N for quinone ligands.

2. Materials and methods

2.1. Materials

Dodecyl maltoside was obtained from Anatrace. DEAE-Biogel and Tween-20 were obtained from Bio-Rad Laboratories. Antimycin, diisopropylfluorophosphate, decyl-ubiquinone and myxothiazol were purchased from Sigma Chemical Co. Dithionite was purchased from Fluka Biochemica. Decyl-ubiquinol was prepared as described before and quantified spectrophotometrically using the reported extinction coefficient [11].

2.2. Purification of cytochrome bc_1 complexes

The yeast strains with the KM91 background and the cytochrome *b* mutants M221Q, M221E and W30C [10,12] were obtained from Dr. Anne-Marie Colson (Universite Catholique de Louvain-La-Neuve, Belgium) and Dr. Gael Brasseur (CNRS Marseille, France). The yeast strains with the W303 background and cytochrome *b* mutants S20T, Q22E, Q22T and L198F were described in Ref. [7]. Cytochrome bc_1 complexes from wild-type yeast and mutant strains were purified as described previously [13]. Cytochrome bc_1 activity was determined in assay buffer containing 50 mM potassium phosphate, pH 7.0, 1 mM sodium azide, 1 mM EDTA and 0.01% Tween-20, using 50 μM decyl-ubiquinol and 50 μM cytochrome *c*. The quantifications of purified enzymes were performed spectrophotometrically as described previously [14], using extinction coefficients of 17.5 mM^{-1} cm^{-1} at 554−539 nm for cytochrome c_1 [15] and 50 mM^{-1} cm^{-1} at 562−578 nm for the combined b_H and b_L hemes in cytochrome *b* [16].

2.3. Pre-steady-state reduction of bc_1 complexes

The reduction of cytochrome *b* and cytochrome c_1 was followed at 24 °C by stopped flow rapid scanning spectroscopy using the OLIS rapid scanning monochromator [14]. Reactions were started by rapid mixing of 2 μM enzyme in assay buffer, containing 0.05% Tween-20, with an equal volume of assay buffer, containing 0.05% Tween-20 and different concentrations of decyl-ubiquinol. Two equivalents of antimycin or myxothiazol were added to the enzyme syringe, if noted. For each experiment, 4–8 data sets were averaged and the oxidized spectrum was subtracted. The kinetic traces were further processed using OLIS software, exported to Origin and manipulated as described previously [4] to obtain the absorbance changes attributable to cytochrome c_1 and cytochrome *b*. The absorbance changes were fitted to either a monophasic or a biphasic exponential function.

2.4. Redox titrations

Potentiometric titrations were performed at 24 °C in a 3.5-ml quartz cuvette, as described previously [17], and the redox status of the *b* hemes was monitored spectrophotometrically. The potential was measured with a platinum–Ag/AgCl (3 M) micro-electrode (MI-80414-6, Microelectrodes, Inc.). All values were expressed with respect to the normal hydrogen electrode (NHE). The electrode was calibrated against a pH 7 standard solution of quinhydrone (Em=+296 mV versus NHE). The purified cytochrome bc_1 complexes were diluted to 2 μM in 50 mM potassium phosphate pH 7 with 0.05% Tween-20. Redox equilibration between the protein and the electrode was achieved by a mixture of the following dyes (with their respective midpoint potential versus NHE at pH 7): 70 μM 2,3,5,6-tetramethyl-*p*-phenylenediamine (+240 mV), 25 μM 1,2-naphtoquinone (+144 mV), 25 μM phenazine methosulfate (+80 mV), 25 μM phenazine ethosulfate (+55 mV), 50 μM duroquinone (+5 mV), 30 μM menaquinone (−76 mV), 50 μM 2-hydroxy-1,4-naphtoquinone (−145 mV), 30 μM anthraquinone-2,6-disulfonate (−184 mV) and 30 μM anthraquinone-2-sulfonate (−225 mV). A 10 or 100 mM solution of dithionite or ferricyanide was used for the reductive and oxidative titrations, respectively. The visible spectra were recorded between 500 and 600 nm. The absorbances at 562−578 nm, after subtracting the oxidized spectrum, were plotted against the potential of the system. The graphed data were fitted to a double $n=1$ Nernst equation, using the Origin program, to obtain the redox potentials for the b_H and b_L hemes [5]. The Nernst plots for the oxidative and reductive titration exhibited no hysteresis, confirming that the system was at equilibrium.

2.5. Molecular modeling

Structural changes associated with the mutations in cytochrome *b* were modeled into the yeast cytochrome bc_1 complex, using the coordinates of the stigmatellin-liganded enzyme (PDB 1EZV, Ref. [6]). Computations were performed on a Silicon Graphics O2™ work-station using programs included in Insight II® (Accelrys, Inc. San Diego). The molecular dynamics and energy minimization calculations were done with the Discover® program, using the CVFF and CFF91 force fields. The modeling focused on the cytochrome *b* subunit of the bc_1 complex, along with associated heme groups and buried water molecules. The heme iron atoms were removed temporarily from the model in order to make the structure compatible with the force fields. The effect of this removal was negligible, as the heavy atoms were located in regions of the molecule that were fixed during simulation. The atomic potentials were then assigned using the automatic function within the Insight II® software.

Mutations were introduced into the cytochrome *b* structure using the Biopolymer® module. Three subsets were created within each structure in order to facilitate modeling. The central subset was left flexible in the key regions near the mutations. Surrounding the flexible subset was a 5-Å radius shell of fixed residues designed to anchor the flexible subset within the larger complex. Finally, the most distant residues were placed in a subset excluded from modeling in order to speed simulation. The flexible subset for the W30C mutant structure consisted of cytochrome *b* residues 17–38 that are part of helix A and the preceding loop region, in addition to a 6-Å radius around Trp-30. This subset was designed to allow the mutated residue a fair amount of freedom in sampling conformational space. Both of the hemes were included in the calculations with their positions fixed. This technique was used in order to accent the structural effects of mutation-induced conformational changes relative to the heme groups.

Following a brief steepest descent minimization, the structure was subjected to a full molecular dynamics simulation. Non-bonding interaction calculations were limited to 9.5 Å, the dielectric constant was set to 2.0, and the temperature held constant at 298 K. Each simulation began with 5000 fs of equilibration using a 1.0 fs per iteration time step and the velocity scaling temperature control method. Molecular dynamics simulation was continued for an additional 50 ps using a 0.5 fs per iteration time step and the more accurate Nosé temperature control method. Successful equilibration was judged by plotting both the running and batch averages for the total energy versus time. Equilibrium was reached when the batch-average energies oscillated smoothly around the constant running-average energy. During molecular dynamics, the structures were saved every 50 fs. Upon reaching equilibrium, the lowest energy structure from each run was selected for a full minimization. Minimization was carried out to a final convergence of 0.001, using the steepest descent, conjugate gradient, and Newton (BFGS) methods in succession. Two runs were performed for the structure of the mutated protein and then compared to the wild-type structure by superposition.

3. Results

3.1. Location of mutations in cytochrome b

The Met-221 and Trp-30 mutations were originally isolated as non-native, intragenic revertants of cytochrome *b* mutations in a KM91 yeast strain. The original M221K mutation [18] resulted in a respiratory deficient phenotype that was corrected by substitution of lysine with glutamate (M221E) or glutamine (M221Q) [9]. The third strain, containing the W30C mutation, was obtained after segregating this mutation from the respiratory competent, but thermo-labile W30C/S206L parent strain [10]. This strain was obtained as a revertant of the S206L strain that had a respiratory-deficient phenotype [18]. The W30C strain grew normally on non-fermentable carbon sources and did not have the thermo-sensitive phenotype of the W30C/S206L parent strain.

The yeast strains containing the cytochrome *b* mutations of Ser-20 (S20T), Gln-22 (Q22T and Q22E) and Leu-198 (L198F) were previously selected for resistance of the W303 parental strain towards the novel center N inhibitor, ilicicolin H [7]. The growth phenotype of the yeast on non-fermentable carbon sources and preliminary biochemical analyses of cytochrome bc_1 complexes in the mitochondrial membranes isolated from these mutants indicated that these mutations had no significant effect on the steady-state activity or stability of the bc_1 complex in the membranes.

The locations of the mutations in center N of cytochrome *b* are shown in Fig. 1. Trp-30 and Leu-198 are in close proximity of both the quinone and the porphyrin rings (Fig. 1A). The tryptophan forms a hydrogen bond with one of the propionate groups of the heme b_H and is highly conserved, as can be seen from the sequence alignments in Fig. 2. Leu-198 is located on the other side of the porphyrin ring, forming a hydrophobic interaction with ubiquinone and the b_H heme. It is also located next to one of the axial ligands to the heme b_H iron, His-197. Leu-198 is only weakly conserved and is replaced by other hydrophobic residues, including isoleucine, phenylalanine and methionine in the cytochrome *b*s from other species (Fig. 2 and Ref. [19]).

The other three residues are located within 5 Å of each other, on the other side of the quinone ring with respect to the b_H heme (Fig. 1B). Met-221 forms a hydrophobic interaction with the ubiquinone. This interaction appears to be highly conserved based on the structures from bovine [20], chicken [21] and *Rhodobacter capsulatus* [22], but the counterpart residue in these and most cytochrome *b*s is a phenylalanine (Fig. 2, Ref. [19]). Ser-20 and Gln-22 appear to be part of a hydrogen bonding network that also includes the active site water, His-202, and one carbonyl groups of the ubiquinone (Fig. 1B). Although these residues are not conserved and are substituted by hydrophobic and aliphatic residues in cytochrome *b*s of other species (Fig. 2, Ref. [19]), their involvement in hydrogen bonding to the active site water may make them of unique importance to quinone binding at center N in the yeast enzyme.

3.2. Effect of cytochrome b mutations on properties of the b hemes

Optical spectra of the cytochrome bc_1 complexes purified from the center N mutants and the wild-type parental strains showed that, with the exception of the L198F mutant, there is no obvious changes in the cytochrome *b* spectral properties as a

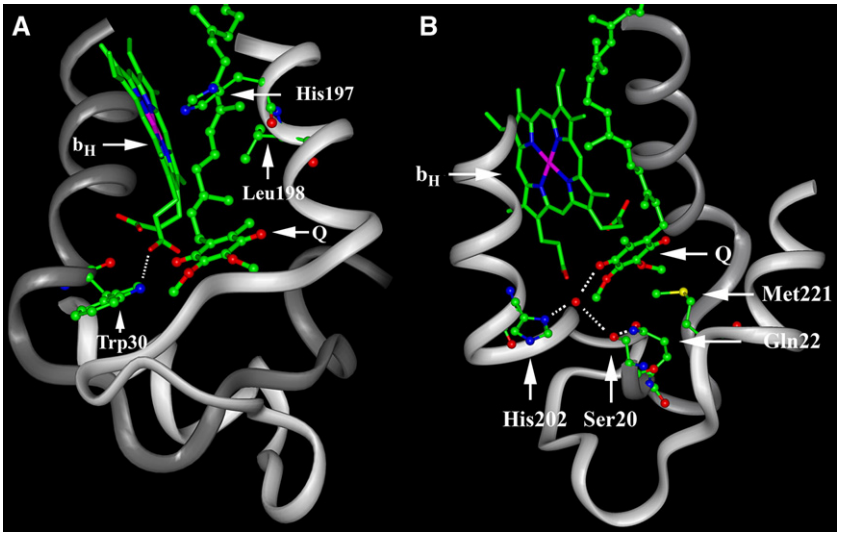

Fig. 1. Views of center N and the location of the center N mutations in relation to the b_H heme and ubiquinone. Panel A shows the location of Trp-30 and Leu-198, which have been mutated in the current study, in relation to the b_H heme ring and ubiquinone (Q) bound at center N. His-197, which is one of the axial heme ligands, is also shown. Panel B shows the location of Ser-20, Gln-22 and Met-221, which are also sites of mutations, in relation to the b_H heme ring and ubiquinone. Also shown is the hydrogen bonded water molecule between Ser-20, His-202 and a carbonyl oxygen on ubiquinone. In both panels carbon atoms are colored green, oxygen atoms are red, nitrogen atoms are blue and the heme iron is pink. The ribbon diagrams show the backbone structure of cytochrome *b* from residues 15-40 and from residues 194–231. Coordinates are from the yeast structure [6] (Protein Data Bank code 1EZV).

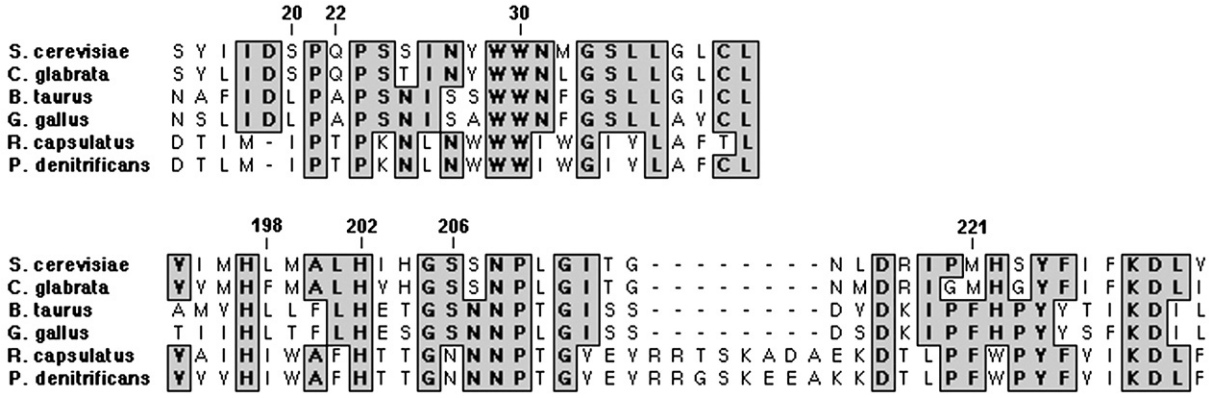

Fig. 2. Sequence alignment of the cytochrome *b* proteins from several species in the regions including residues 15–40 and 194–231 forming the ubiquinone reduction pocket at the center N site. The alignment was constructed using ClustalW and yeast numbering. The numbered lines show the positions of the center N mutations that were analyzed, plus His-202 and Ser-206. The species are *Saccharomyces cerevisiae*, *Candida glabrata*, *Bos taurus*, *Gallus gallus*, *Rhodobacter capsulatus*, and *Paracoccus denitrificans*.

consequence of the mutations or genetic background of the wild-type parental strain. The α-band of the reduced cytochrome *b* is at 562 nm and there is no change in the b:c_1 ratio of 2 to 1 (results not shown). The L198F mutation has a hypsochromic effect on the α-band, shifting it by ~0.5 nm (Fig. 3). The resulting difference spectrum of the L198F and wild-type enzymes has a peak at 559 and a trough at 564 nm (Fig. 3). Assuming the same ratio of *b* hemes to cytochrome c_1, the extinction coefficient for the *b* hemes appears not to be changed.

The redox midpoint potentials of the two *b* hemes that were determined by potentiometric titration at pH 7 and monitored spectrophotometrically are presented in Table 1. With the bc_1 complex from the two wild-type parental strains we obtained midpoint potentials of ~80 mV and ~−56 mV for the b_H and b_L heme, respectively (Fig. 4). Within the experimental error of the methodology, the midpoint potentials of the b_H and b_L hemes in five of the seven mutants, M221E, M221Q, Q22E, Q22T and L198F, are very similar or changed only a small amount compared to those of the *b* hemes in the wild-type enzymes (Fig. 4, Table 1). Surprisingly the S20T mutation also induces a small shift in the redox potential of both *b* hemes, although this residue is not in close contact with either heme. Apparently this mutation has some long-range structural effects that impact the thermodynamic properties of the b_H and b_L hemes.

The bc_1 complex from the W30C mutant also shows a clear shift in its potentiometric titration curve (Fig. 4B), decreasing the

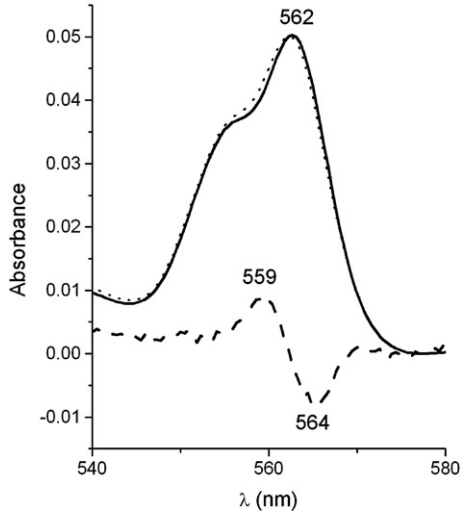

Fig. 3. Absorption spectra of reduced minus oxidized cytochrome bc_1 complexes from wild-type yeast and the L198F mutant. Spectra were recorded before and after reduction of 1 μM enzyme with dithionite. The solid line is the spectrum of the enzyme from wild-type yeast (W303 strain) and the dotted line is of the L198F mutant enzyme. The dashed line shows the difference spectrum of the L198F mutant enzyme minus the spectrum of the bc_1 complex from wild-type yeast, expanded by a factor of five.

Table 1
Ubiquinol–cytochrome *c* reductase activities and redox midpoint potentials for the *b* hemes of the bc_1 complexes from wild-type yeast strains and center N mutants

Strain	TN (s^{-1}) [b]	E_{m7} (mV) [a]	
		b_L	b_H
KM91 background			
KM91(wild type)	150–180	−53	+79
M221Q	90–150	−47	+76
M221E	120–180	−63	+63
W30C	140–170	−58	+32
		−34 [c]	+53 [c]
W303 background			
W303 (wild type)	200–290	−60	+82
S20T	140	−70	+59
Q22T	230–250	−56	+70
Q22E	260	−60	+77
L198F	260	−60	+80

Experimental conditions are described in Materials and methods.

[a] Values are for the reductive titration with the trace for the oxidative titration very similar to the reductive titration. Data were fitted to a double Nernst function with the b_H heme contributing ~70% and the b_L heme ~30% to the total absorbance of the *b* heme at 562 nm, as described in Materials and methods.

[b] TN = turn-over number.

[c] Data were fitted to a double Nernst function with b_H and b_L heme contributing equally to the total absorbance of the *b* heme at 562 nm.

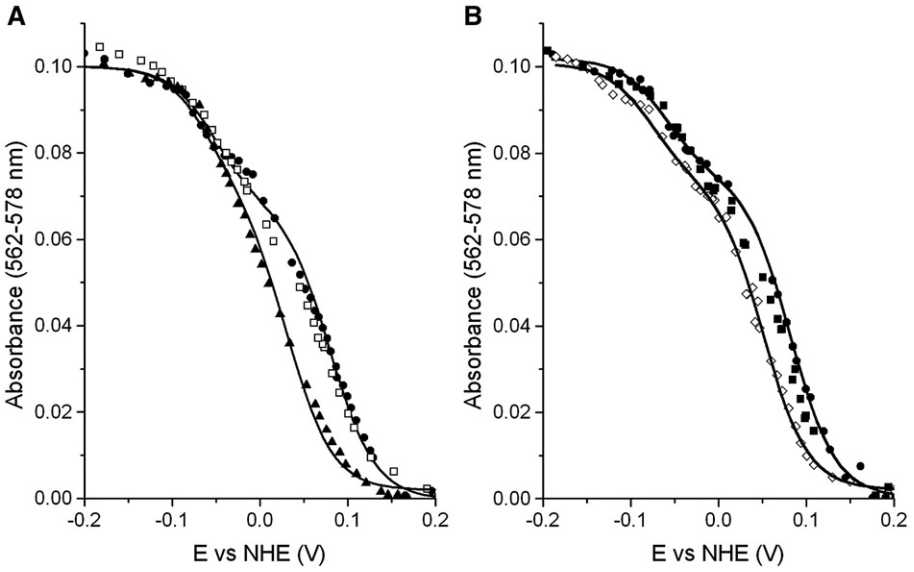

Fig. 4. Potentiometric titrations of the *b* hemes in wild-type cytochrome bc_1 complex and bc_1 complexes from the center N mutants. Potentiometric titrations were performed at pH 7 and the redox status of the *b* hemes was monitored spectrophotometrically, as described under Materials and methods. Panel A shows the curves for reductive redox titrations of the *b* hemes in bc_1 complexes from the KM91 wild-type strain (closed circle), and the M221Q (open square) and W30C (closed triangle) mutants. Panel B shows the heme *b* titrations curves of the bc_1 complexes from the W303 wild-type strain (closed circle), and the L198F (closed triangle) and S20T (open diamond) mutants. The solid lines in panels A and B are the fits to a double Nernst function with the b_L and b_H heme contributing ~30 and ~70%, respectively, to the total heme *b* absorbance. The complete data set of absorbance versus wavelength at different redox potentials for the KM91 wild-type and W30C enzymes are available as Supplemental data, Tables 1 and 2, respectively.

difference in midpoint potential between the two heme *b*s by ~40 mV. The best fit to a double Nernst function was obtained when it was assumed that the b_H and b_L hemes contribute equally to the total absorbance at 562−578 nm, which is different from the 70:30 ratio in the other bc_1 complexes. This fit calculates a decrease in the midpoint potential of the b_H heme by ~20 mV and an increase of the b_L heme by ~20 mV. On the other hand, fixing the contribution of b_H heme at 70% also gives a satisfying fit. In this case the redox midpoint potential of the b_L heme is similar to the other bc_1 complexes and the b_H heme is

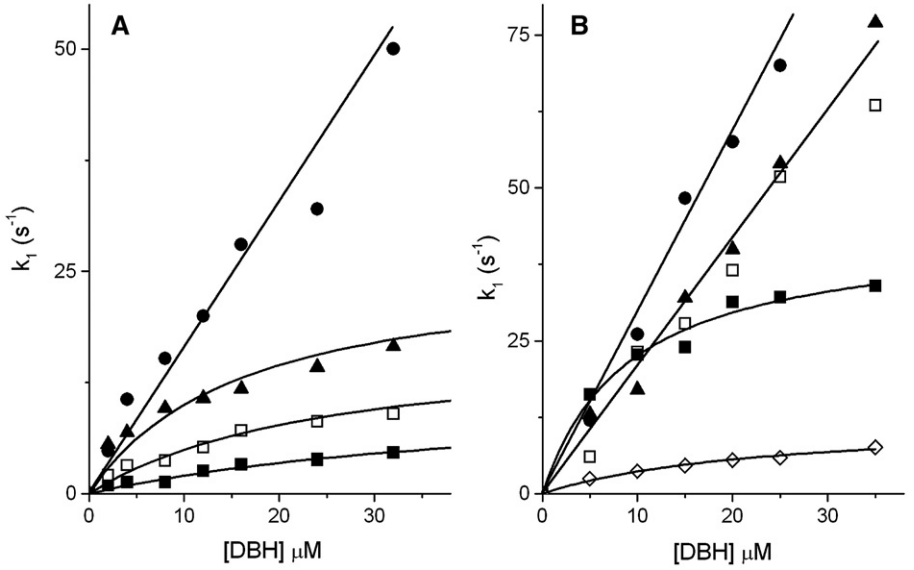

Fig. 5. Dependence of pre-steady-state cytochrome *b* reduction rates on decyl-ubiquinol concentration in the presence of myxothiazol. Panels A and B show the rates of the first (fast) phase of cytochrome *b* reduction in the cytochrome bc_1 complexes from wild-type yeast and center N mutants with the KM91 and W303 backgrounds, respectively. In panel A, rates for the KM91 wild-type enzyme are represented by solid circles, M221E by open squares, M221Q by solid squares, and W30C by solid triangles. In panel B, rates for the W303 wild-type enzyme are represented by solid circles, S20T by open diamonds, Q22T by open squares, Q22E by closed squares, and L198F by closed triangles.

decreased by ~40 mV to +32 mV. The difference in the two calculated fittings is discussed further below.

3.3. Effect of cytochrome b mutations on steady-state kinetic properties of the bc_1 complex

Cytochrome *c* reductase activities of the purified cytochrome bc_1 complexes from the two wild-type strains and the center N mutant strains are shown in Table 1. Variable delipidation during purification is probably responsible for the variability in steady-state activities from different batches, but in each genetic background, most of the mutants exhibit close to wild-type activity. The one exception is the bc_1 complex with the S20T mutation, which decreases the turnover number by ~50%. None of the mutations affected the dependence of the activity on decyl-ubiquinol concentration, with an apparent K_m of ~10 μM for all of the isolated enzymes (results not shown).

3.4. Effect of cytochrome b mutations on the pre-steady-state reduction of the b hemes through center N

Myxothiazol blocks quinol oxidation at center P, preventing reduction of the high potential chain, the Rieske iron–sulfur cluster and cytochrome c_1, but the low potential chain, cytochrome *b*, can still be reduced by decyl-ubiquinol through center N. This makes it possible to study specifically the effects of the center N mutations on the electron transfer reaction through the quinone reduction site. Fig. 5 shows the rates of the first (fast) reduction phase of the *b* hemes as a function of decyl-ubiquinol concentration. The results in panel A show that the mutations of Met-221 and Trp-30 decrease the rate of heme *b*

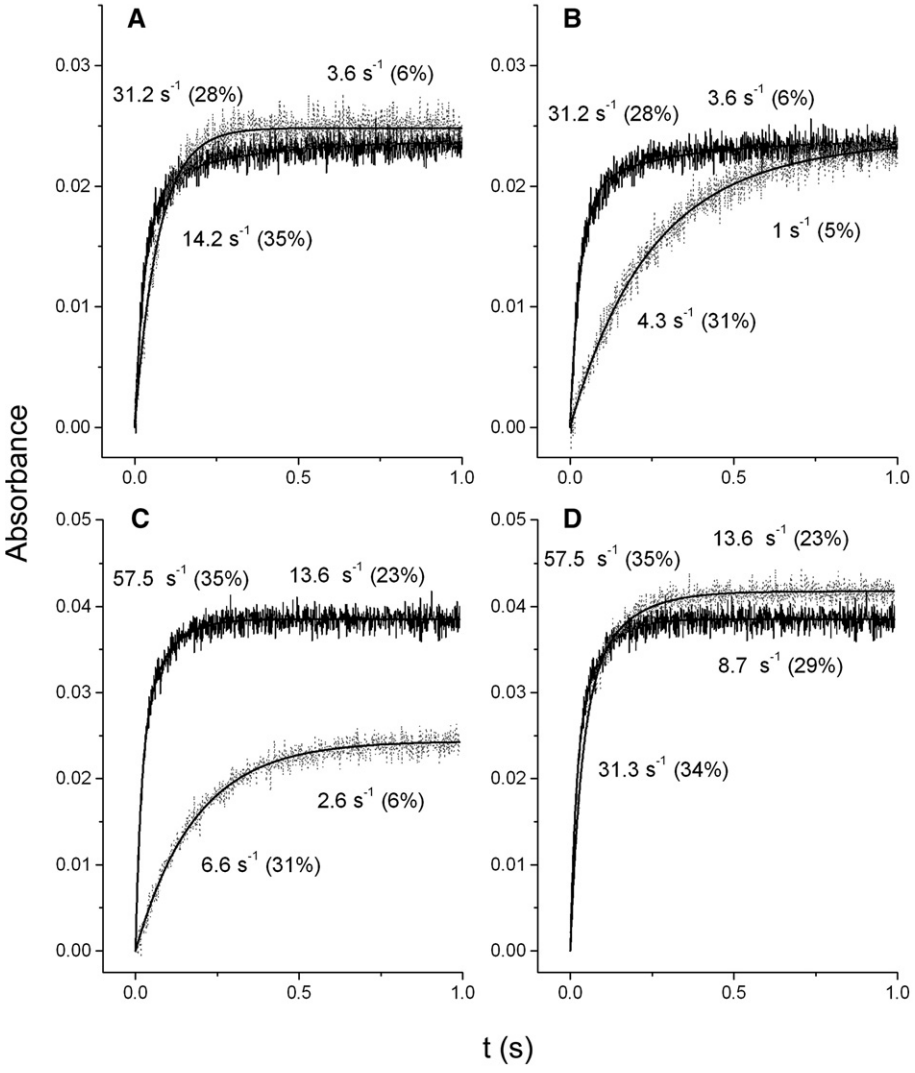

Fig. 6. Pre-state reduction of cytochrome *b* by decyl-ubiquinol in the presence of myxothiazol. The traces in panels A and B show the reduction of cytochrome *b* in the cytochrome bc_1 complex from the KM91 wild-type yeast strain (black), and the bc_1 complexes from the M221E (grey, panel A) and W30C (grey, panel B) mutant strains upon mixing with 24 μM decyl-ubiquinol. Panels C and D show the reduction of cytochrome *b* in the cytochrome bc_1 complex from the W303 wild-type strain (black), and S20T (grey, panel C) and Q22E (grey, panel D) mutant strains reduced with 20 μM decyl-ubiquinol. The traces were fitted to a monophasic or biphasic function. Rates and extent of reduction of the b_H heme (%) are indicated for each trace, with values for the enzymes from the wild-type strains shown above the traces and values for the enzymes from the mutants shown below the traces.

reduction significantly in comparison to the rate of the enzyme from the KM91 wild-type strain. While the rates for the enzyme from the wild-type strain are non-saturating over the range of decyl-ubiquinol concentration measured, the rates for the enzymes from the Met-221 and Trp-30 mutants deviate from a linear relationship as the concentration increases. All of the mutations to Ser-20, Gln-22, and Leu-198 also affect the rate of *b* heme reduction compared to the rate with the enzyme from the W303 wild-type strain (Fig. 5B), with the most pronounced decrease caused by the S20T mutation. The rates are non-saturating for the W303 wild-type enzyme as the concentration of decyl-ubiquinol increases, as well as for the enzyme from the Q22T and L198F mutants, while the rates of the Q22E and S20T enzymes saturate at the higher concentrations.

Fig. 6 shows representative kinetic traces for reduction of cytochrome *b* through center N in the bc_1 complexes from the M221E and W30C mutants compared to the KM91 wild-type enzyme, and from the S20T and Q22E mutants compared to the W303 wild-type enzyme. With the exception of the enzyme with the W30C mutation in cytochrome *b*, all of the curves could only be fitted to two phases. Most of the center N mutations, with the exception of S20T, appear to have no significant effect on the total extent of reduction, including the M221Q, Q22T and L198F mutations (data not shown), while all of the mutations affect the rate of *b* reduction to differing extents. The S20T cytochrome *b* mutation has the most profound effects, causing an ~40% decrease in extent and ~90% decrease in rate of cytochrome *b* reduction compared to the enzyme from the W303 wild-type yeast (Fig. 6C). These changes, combined with the effects on the midpoint potentials of both *b* hemes noted above suggest that this mutation extensively damages the bc_1 complex. Whereas the ~50% decrease in rate of cytochrome *b* reduction resulting from the W30C mutation (Fig. 6B) is consistent with the change in midpoint potential of the b_H heme in this enzyme, the decreased rates resulting from the M221E (Fig. 6A) and Q22E (Fig. 6D) mutations cannot be explained on thermodynamic grounds. These are discussed in more details below.

3.5. Effect of cytochrome b mutations on the pre-steady-state reduction of b and c_1 hemes through center P

To probe the influence of the center N mutations on the quinol oxidation reaction at center P, pre-steady-state reduction studies were performed in the presence of antimycin to block reduction of the *b* hemes through center N. Kinetic traces for reduction of the cytochrome bc_1 complexes from the wild-type strains and six selected mutants are shown in Fig. 7. The rates of reduction of the *b* and c_1 hemes in most of the mutant enzymes are similar to those in the bc_1 complexes from the wild-type strains. Subtle changes are observed for the W30C mutant, with a 50% increase in the rate of heme c_1 reduction. There was also a ~50% decrease in rates of heme c_1 and *b* reduction in the enzyme with the S20T mutation, which is consistent with the comparable drop in catalytic activity of this enzyme (Table 1). The extent of reduction of heme *b* and heme c_1 varies among the bc_1 complexes from the wild-type strains and the mutants. However, the ratios of the extent of reduction of c_1 and *b* hemes for the different enzymes are very similar, ~0.55. This indicates that the mutations and the genetic background of the wild-type yeast strain have no effect on the redox equilibrium between the Rieske center and the c_1 heme.

4. Discussion

In the current study we have examined the kinetic and thermodynamic properties of the cytochrome bc_1 complexes from seven yeast strains with mutations in the vicinity of center N [7,9,10]. Based on their location in relation to the ubiquinone binding pocket and/or the b_H heme we expected that these mutations might affect center N kinetics. Trp-30 is highly conserved in bacterial and mitochondrial cytochrome bc_1 complexes and forms a hydrogen bond with the propionate side group of the b_H heme (Fig. 1A). A hydrophobic interaction of the ubiquinone with Met-221 appears also to be highly conserved (Fig. 1A). Ser-20, Gln-22 and Leu-198, however, are not conserved (Fig. 2). In the yeast structure, Leu-198 is in close proximity of both the b_H heme and ubiquinone. Ser-20 and Gln-22 are within 5 Å of the ubiquinone ring and in close proximity of Met-221. Ser-20 and Gln-22 also form a hydrogen-bonding network that includes His-202, one of the carbonyl groups of the ubiquinone ring, and an active-site water that is present in the yeast structure but not in the structure from other species (Fig. 1B).

The steady-state activities of bc_1 complexes from the center N mutants, with the exception of the S20T mutant, are very similar to the activities of the enzymes of the wild-type yeast they were derived from (Table 1). This is in agreement with the growth phenotype on a non-fermentable carbon source and the cytochrome *c* reductase activities of mitochondrial membranes isolated from these mutants [7,9,10]. On the other hand, the S20T mutation results in a 50% decrease in the turnover number in a catalytic assay (Table 1) and significant decrease in pre-steady-state kinetics through both center N (Fig. 6) and center P (Fig. 7), although its growth phenotype and mitochondrial cytochrome *c* reductase activity were comparable to those of the wild-type yeast [7]. This indicates that solubilization with detergent and column purification have global structural effects on the enzyme of this mutant.

The mutation of leucine to a phenylalanine at position 198 (L198F) induces a small blue-shift in the maximum of the α-band of the reduced cytochrome *b* (Fig. 3), indicating that the bulkier hydrophobic residue alters the electronic environment around the b_H heme. This could occur through a direct interaction with the heme macrocycle, as is observed with the center N inhibitors, antimycin or ilicicolin, binding of which near the tetrapyrole ring also results in a shift in the absorbance maximum [23,24]. Alternatively, the mutation might have an indirect effect on the histidine ligand to the heme iron, His-197. The orientation of the axial imidazole ligand planes has been proposed to play a significant role in modulating heme iron d_π orbital energy levels [25]. A hydrophobic interaction with phenylalanine may have changed this orientation. However, the structural change seems to be subtle, based on the absence of a

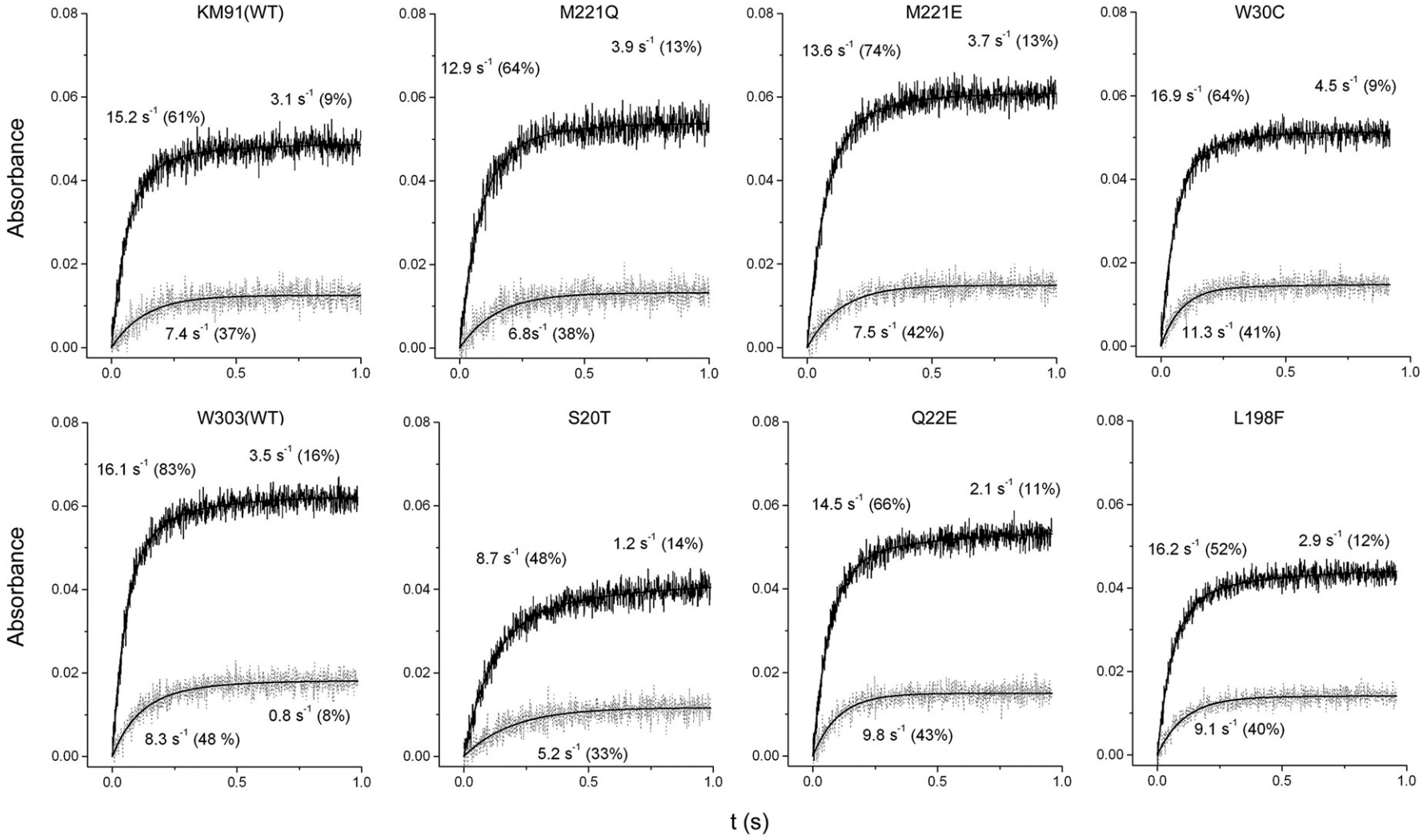

Fig. 7. Pre-steady-state reduction of cytochrome *b* and cytochrome c_1 by decyl-ubiquinol in the presence of antimycin. The top panels show the kinetic traces for the cytochrome bc_1 complexes from the KM91 wild-type strain, and the M221Q, M221E and W30C mutant strains. In these experiments 1 μM enzyme was reduced with 24 μM decyl-ubiquinol. The bottom panels show the kinetic traces for the cytochrome bc_1 complexes from the W303 wild-type strain, and the S20T, Q22E and L198F mutant strains. In these experiments 1 μM enzyme was reduced with 20 μM decyl-ubiquinol. The traces show cytochrome c_1 reduction in gray and cytochrome *b* reduction in black. Rates and extent of reduction are indicated for each trace, with values for b_H heme reduction shown above the traces, and values for cytochrome c_1 reduction shown below.

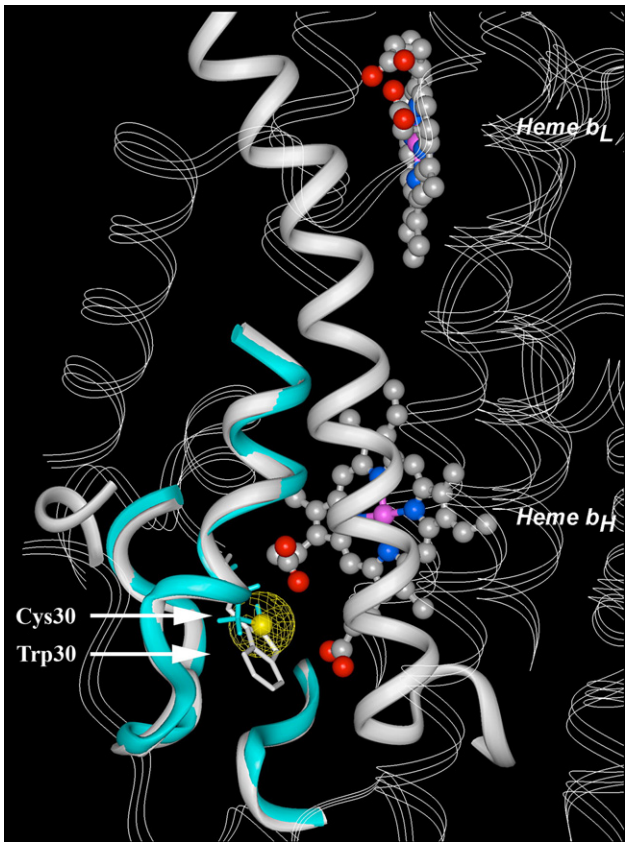

Fig. 8. Structural changes resulting from the W30C cytochrome *b* mutation. The figure shows the location of the W30C mutation in the non-helical region of cytochrome *b* preceding helix A, proximal to heme b_H. The calculated structure of the non-helical region preceding helix A in the W30C mutant is colored turquoise and overlaid on the structure of the non-helical region from the wild-type enzyme. Trp-30 from the wild-type cytochrome *b* and Cys-30 from the mutant are displayed simultaneously and labeled.

change in the thermodynamic properties of the *b* hemes (Fig. 3, Table 1) and only a small decrease in center N kinetics (Figs. 5, 6). Indeed, sequence analysis of the cytochrome *b* genes across species shows that this residue is substituted by other larger apolar residues, for example, a phenylalanine in *C. glabrata* or isoleucine in *R. capsulatus* (Fig. 2).

In the W30C mutant, the spectral features of the combined *b* hemes appear not to be altered, but the thermodynamic properties have changed. A shift in the redox midpoint potential of the b_H heme is obvious (Fig. 4A). Part of this change may result from the larger van der Waals radius of the sulfur compared to nitrogen, which has the effect of increasing electron density proximal to the heme ring, as shown in Fig. 8. In addition, the hydrogen bond between the nitrogen from the indole ring of the tryptophan is lost, and modeling of the cysteine substitution into the crystal structure of the yeast bc_1 complex, followed by energy minimization of the altered structure, suggests that the cysteine sulfur may interact with the carboxylate group of a propionate on the porphyrin ring (Fig. 8). Additional interactions that are not shown by our calculations may accommodate the loss of the large indole side-chain of the tryptophan. The result of these structural changes is either a more stable oxidized heme iron, or a less stable reduced heme iron, thus lowering the redox potential of the b_H heme.

When the potentiometric titration curve for the enzyme with the W30C mutation was fitted to a double Nernst equation the best fit was obtained with both *b* hemes contributing equally to the total absorbance of cytochrome *b*. This would suggest that the W30C mutation has a long-range electronic effect on both the b_H and b_L heme. This fit also suggests that the midpoint potential of both the b_L and b_H heme has changed, by approximately +20 mV and −20 mV, respectively, suggesting redox interaction between the hemes. This long-range thermodynamic effect on the heme near the quinol oxidation site at center P may have modulated the kinetics of the bifurcated reaction, since a small increase in the rate of cytochrome c_1 reduction through center P was observed (Fig. 7). On the other hand, a slightly less satisfactory fit could be obtained by fixing the contribution of the b_L and b_H heme at 30 and 70%, respectively, implying that there is no long-range thermodynamic effect. In this case the midpoint potential of the b_H heme is decreased by ~40 mV, while the b_L heme is unchanged. Regardless of which fit is used, the lower thermodynamic driving force between the decyl-ubiquinol substrate and the b_H heme can readily explain the slower reduction kinetics of the b_H heme through center N (Figs. 5, 6).

The midpoint potentials of the b_H and b_L heme in the bc_1 complexes with mutations of Met-221 and Gln-22 were unchanged (Table 1). This was expected, considering the location of these residues, approximately 7 Å away from the b_H heme (Fig. 1B). Thus, the slowing in center N kinetics (Figs. 5, 6) can be attributed to a change in the affinity of this site for the quinol ligands and a pronounced drop in electron transfer rate, possibly due to a change in electron transfer distance. Interestingly, the total extent of reduction is not significantly different from that of the wild-type enzyme, even for the M221E mutant that is the most severely impaired in center N kinetics. This suggests that the thermodynamic properties of the quinone are not perturbed and that the binding geometry of quinone species has changed, thus increasing the distance parameter for electron transfer. In the M221Q and M221E mutants, the hydrophobic interaction with the quinone is obviously lost and the replacement of methionine with smaller residues widens the binding pocket. In the bc_1 complex from *R. capsulatus*, the loss of the hydrophobic interaction by a F244L mutation, introducing a smaller isoleucine near the ubiquinone ring, resulted in an enzyme that was not assembled or highly unstable [26]. This suggests that in the yeast mutant enzymes, the glutamate and glutamine form new interactions to stabilize the enzyme. Moreover, center N still has a significant high affinity for the decyl-ubiquinol substrate (Fig. 5) and an alternative binding conformation with a larger distance between the quinone ring and b_H heme may explain the slower kinetics. The introduction of a larger, positively charged lysine residue, as in the respiratory deficient M221K strain blocked center N kinetics completely [12]. One possible explanation is that the lysine residue prevents binding of ubiquinone. Indeed, this mutation abolished binding of antimycin, a strong center N inhibitor [12].

The effect on the center N kinetics due to the two Gln-22 mutations varies. The kinetics for the Q22T enzyme are very similar to those of the wild-type enzyme (Figs. 5, 6). This is somewhat surprising because this mutation may break the hydrogen-bonding network around the active site water (Fig. 1B) and open up the pocket around this residue. The high substrate affinity suggests either that the hydrogen-bonded water is not lost or is not critical for substrate binding, or the loss of the hydrogen bond is compensated by new or existing interactions. The Q22E substitution has a more dramatic effect on the center N kinetics, possibly because the introduction of the more electronegative glutamate residue near the ubiquinone ring may destabilize the anionic semiquinone at center N.

The S20T mutation compromises both the rate and extent of heme *b* reduction through center N (Figs. 5, 6). The affinity of center N for quinone ligands is changed due to the S20T mutation and probably plays the main role in the slower rate of electron transfer through center N. Although the hydroxyl group on the threonine may still be able to form a hydrogen bond with the active site water in a similar orientation, the methyl group will clash with Met-221. Thus subtle conformational changes are required to accommodate this mutation, either by changing the hydrogen-bonding network or reorienting the Met-221 and its interaction with the ubiquinone.

The effect of the S20T mutation extends beyond center N. The rates of reduction of *b* and c_1 hemes through center P dropped by ~50%, which correlates with the drop in cytochrome *c* reductase activity (Table 1). The lower extent of reduction (Fig. 6) further suggests that the Rieske subunit has been partly lost from this enzyme, and this is supported by the titration curve for inhibition by stigmatellin (see Supplemental data, Fig. 1. Interestingly, binding of ligand at center N has previously been shown to have affects on the Rieske subunit accessibility to protease at center P [27]. Considering the normal wild-type activity of the S20T mutant in the membrane, we conclude that the S20T mutation makes the enzyme more susceptible to degradation upon treatment with detergent. Another ilicicolin H resistant yeast strain with a leucine substitution at position 20 contained a labile bc_1 complex in the membrane and exhibited a 50% decrease in cytochrome *c* reductase activity [7]. Interestingly, a leucine residue naturally occurs in cytochrome *b* from chicken and bovine, and another hydrophobic residue, isoleucine, in cytochrome *b* from bacteria (Fig. 2, Ref. [19]). The crystal structures of the bc_1 complexes from these species [20–22] show the loss of the active-site water and rotation of the histidine towards the ubiquinone ring. This configuration is stabilized by a direct hydrogen bond between the histidine and the carbonyl group on the ring, and possibly also by an interaction with leucine or isoleucine in these bc_1 complexes. Our data suggest that structural differences around His-202 (yeast sequence) are important for optimal center N kinetics and stability of the bc_1 complexes from different species.

In conclusion, the center N mutants characterized here show that lowering the redox potential of the b_H heme and, moreover, expansion of the volume within center N slows down electron transfer between quinol and the b_H heme. Therefore, conserving a narrow volume within the center N pocket appears to be an important factor to allow fast electron transfer between the quinone ligands and the b_H heme, as well as to promote the formation of the semiquinone intermediate [28].

Acknowledgement

This research was supported by NIH research grant GM 20379.

Appendix A. Supplementary data

Supplementary data associated with this article can be found, in the online version, at doi:10.1016/j.bbabio.2007.08.005.

References

[1] B.L. Trumpower, R.B. Gennis, Energy transduction by cytochrome *c*omplexes in mitochondrial and bacterial respiration: the enzymology of coupling electron transfer reactions to transmembrane proton translocation, Annu. Rev. Biochem. 63 (1994) 675–716.
[2] P. Mitchell, Possible molecular mechanisms of the protonmotive function of cytochrome systems, J. Theor. Biol. 62 (1976) 327–367.
[3] R. Covian, B.L. Trumpower, Rapid electron transfer between monomers when the cytochrome bc_1 complex dimer is reduced through center N, J. Biol. Chem. 280 (2005) 22732–22740.
[4] R. Covian, E.B. Gutierrez-Cirlos, B.L. Trumpower, Anti-cooperative oxidation of ubiquinol by the yeast cytochrome bc_1 complex, J. Biol. Chem. 279 (2004) 15040–15049.
[5] R.G. Covian, K. Zwicker, F.A. Rotsaert, B.L. Trumpower, Asymmetric and redox-specific binding of quinone and quinol at center N of the dimeric yeast cytochrome bc_1 complex: consequences for semiquinone stabilization, J. Biol. Chem 282 (2007) 24198–24208.
[6] C. Hunte, J. Koepke, C. Lange, T. Rossmanith, H. Michel, Structure at 2.3 A resolution of the cytochrome bc_1 complex from the yeast *Saccharomyces cerevisiae* co-crystallized with an antibody Fv fragment, Structure 8 (2000) 669–684.
[7] M.G. Ding, J.P. di Rago, B.L. Trumpower, Investigating the Qn site of the cytochrome bc_1 complex in *Saccharomyces cerevisiae* with mutants resistant to ilicicolin H, a novel Qn site inhibitor, J. Biol. Chem. 281 (2006) 36036–36043.
[8] G. Brasseur, A.S. Saribas, F. Daldal, A compilation of mutations located in the cytochrome *b* subunit of the bacterial and mitochondrial bc_1 complex, Biochim. Biophys. Acta 1275 (1996) 61–69.
[9] J.Y. Coppee, N. Tokutake, D. Marc, J.P. di Rago, H. Miyoshi, A.M. Colson, Analysis of revertants from respiratory deficient mutants within the center N of cytochrome *b* in *Saccharomyces cerevisiae*, FEBS Lett. 339 (1994) 1–6.
[10] G. Brasseur, J.Y. Coppee, A.M. Colson, P. Brivet-Chevillotte, Structure–function relationships of the mitochondrial bc_1 complex in temperature-sensitive mutants of the cytochrome *b* gene, impaired in the catalytic center N, J. Biol. Chem. 270 (1995) 29356–29364.
[11] B.L. Trumpower, C.A. Edwards, Purification of a reconstitutively active iron–sulfur protein (oxidation factor) from succinate. cytochrome *c* reductase complex of bovine heart mitochondria, J. Biol. Chem. 254 (1979) 8697–8706.
[12] G. Brasseur, P. Brivet-Chevillotte, Characterization of mutations in the mitochondrial cytochrome *b* gene of *Saccharomyces cerevisiae* affecting the quinone reductase site (QN), Eur. J. Biochem. 230 (1995) 1118–1124.
[13] C.H. Snyder, B.L. Trumpower, Ubiquinone at center N is responsible for triphasic reduction of cytochrome *b* in the cytochrome bc_1 complex, J. Biol. Chem. 274 (1999) 31209–31216.
[14] C. Snyder, B.L. Trumpower, Mechanism of ubiquinol oxidation by the cytochrome bc_1 complex: pre-steady-state kinetics of cytochrome bc_1 complexes containing site-directed mutants of the Rieske iron–sulfur protein, Biochim. Biophys. Acta 1365 (1998) 125–134.

[15] C.A. Yu, L. Yu, T.E. King, Preparation and properties of cardiac cytochrome c_1, J. Biol. Chem. 247 (1972) 1012–1019.
[16] J.A. Berden, E.C. Slater, The reaction of antimycin with a cytochrome *b* preparation active in reconstitution of the respiratory chain, Biochim. Biophys. Acta 216 (1970) 237–249.
[17] P.L. Dutton, Redox potentiometry: determination of midpoint potentials of oxidation-reduction components of biological electron-transfer systems, Methods Enzymol. 54 (1978) 411–435.
[18] D. Lemesle-Meunier, P. Brivet-Chevillotte, J.P. di Rago, P.P. Slonimski, C. Bruel, T. Tron, N. Forget, Cytochrome *b*-deficient mutants of the ubiquinol–cytochrome *c* oxidoreductase in *Saccharomyces cerevisiae*. Consequence for the functional and structural characteristics of the complex, J. Biol. Chem. 268 (1993) 15626–15632.
[19] M.D. Esposti, S. De Vries, M. Crimi, A. Ghelli, T. Patarnello, A. Meyer, Mitochondrial cytochrome *b*: evolution and structure of the protein, Biochim. Biophys. Acta 1143 (1993) 243–271.
[20] S. Iwata, J.W. Lee, K. Okada, J.K. Lee, M. Iwata, B. Rasmussen, T.A. Link, S. Ramaswamy, B.K. Jap, Complete structure of the 11-subunit bovine mitochondrial cytochrome bc_1 complex, Science 281 (1998) 64–71.
[21] Z. Zhang, L. Huang, V.M. Shulmeister, Y.I. Chi, K.K. Kim, L.W. Hung, A. R. Crofts, E.A. Berry, S.H. Kim, Electron transfer by domain movement in cytochrome bc_1, Nature 392 (1998) 677–684.
[22] E.A. Berry, L.S. Huang, L.K. Saechao, N.G. Pon, M. Valkova-Valchanova, F. Daldal, X-ray structure of *Rhodobacter capsulatus* cytochrome bc_1: comparison with its mitochondrial and chloroplast counterparts, Photosynth. Res. 81 (2004) 251–275.
[23] Y. Kamensky, A.A. Konstantinov, W.S. Kunz, S. Surkov, Effects of bc_1-site electron transfer inhibitors on the absorption spectra of mitochondrial cytochromes *b*, FEBS Lett. 181 (1985) 95–99.
[24] E.B. Gutierrez-Cirlos, T. Merbitz-Zahradnik, B.L. Trumpower, Inhibition of the yeast cytochrome bc_1 complex by ilicicolin H, a novel inhibitor that acts at the Qn site of the bc_1 complex, J. Biol. Chem. 279 (2004) 8708–8714.
[25] M.K. Safo, G.P. Gupta, F.A. Walker, W.R. Scheidt, Models of the cytochromes *b*. Control of axial ligand orientation with a hindered porphyrin system, JACS 113 (1991) 5497–5500.
[26] A. Crofts, B. Hacker, B. Barquera, C.H. Yun, R. Gennis, Structure and function of the *bc*-complex of *Rhodobacter sphaeroides*, Biochim. Biophys. Acta 1101 (1992) 162–165.
[27] J.W. Cooley, T. Ohnishi, F. Daldal, Binding dynamics at the quinone reduction (Qi) site influence the equilibrium interactions of the iron sulfur protein and hydroquinone oxidation (Qo) site of the cytochrome bc_1 complex, Biochemistry 44 (2005) 10520–10532.
[28] V.P. Shinkarev, Ubiquinone (coenzyme Q10) binding sites: low dielectric constant of the gate prevents the escape of the semiquinone, FEBS Lett. 580 (2006) 2534–2539.